

Radio Observations of the Marano Field and the Faint Radio Galaxy Population

C. Gruppioni,^{1,2*} G. Zamorani,^{3,2} H.R. de Ruiter,^{3,2} P. Parma,²
M. Mignoli,³ and C. Lari,²

¹*Dipartimento di Astronomia, Università di Bologna, via Zamboni 33, I-40126 Bologna, Italy*

²*Istituto di Radioastronomia del CNR, via Gobetti 101, I-40129 Bologna, Italy*

³*Osservatorio Astronomico di Bologna, via Zamboni 33, I-40126 Bologna, Italy*

Accepted 1996 November 21. Received 1996 July 26

ABSTRACT

Radio surveys with the Australia Telescope Compact Array have been carried out at 1.4 and 2.4 GHz with a limiting flux of ~ 0.2 mJy at each frequency in the *Marano Field*, in which deep optical and X-ray (ROSAT) data are also available. In this paper we present the two radio samples, complete at the $5\sigma_{local}$ level, consisting of 63 and 48 sources respectively at 1.4 and 2.4 GHz. The 1.4 GHz normalized differential source counts show a flattening below about one mJy, in agreement with the results from previous surveys. The 2.4 GHz counts, which are the deepest at this or similar frequencies (e.g. 2.7 GHz), agree well with the 2.7 GHz counts at higher fluxes and with the extrapolations down to ~ 2 mJy based on fluctuation analyses.

The 2.4–1.4 GHz spectral index distributions are presented for both the complete samples in two flux density intervals. The median spectral index for the 1.4 GHz sample remains constant at $\alpha \sim 0.8$, down to the lowest fluxes ($S_{1.4} \simeq 0.2$ mJy), while for the higher frequency sample the spectral index distribution flattens in the lower flux density interval ($S_{2.4} < 0.8$ mJy). A significant number of sources with inverted spectrum ($\alpha < 0$) does appear in both samples, at low flux level ($\lesssim 2$ mJy). These sources, which are about 25% of the complete sample at 2.4 GHz, are probably the “bright” counterpart of the inverted spectrum sources which appear to be almost 50% of the sources in the even deeper radio surveys (at ~ 20 – 40 μ Jy).

1 INTRODUCTION

Deep multi-frequency radio source counts, together with optical photometric and spectroscopic identifications, are necessary to understand the properties and the cosmological evolution of the faint radio source populations. Deep 1.4 GHz counts show a change in slope below a few milliJansky (mJy), corresponding to a more rapid increase in the number of faint sources (Windhorst 1984; Windhorst et al. 1985). This change in slope has been confirmed by independent surveys of the same areas (Oort & Windhorst 1985) and of different areas (Condon & Mitchell 1984; Oort 1987). A similar change in slope below a few mJy is visible also at other frequencies, e.g. at 5 GHz (Kellerman et al. 1986; Fomalont et al. 1991) and at 8.44 GHz (Windhorst et al. 1993). It is well known that the

fraction of sources identified with elliptical galaxies and quasars, which are the dominant populations in bright radio samples, decreases significantly at these faint fluxes. Various models for different classes of objects, with or without evolution, have been developed in the recent literature to explain the observed sub-mJy counts. Evolving models include normal spiral galaxies (Condon 1984, 1989) or actively star-forming galaxies (Windhorst 1984; Kron, Koo & Windhorst 1985; Windhorst et al. 1985, 1987; Oort 1987; Rowan–Robinson et al. 1993). Wall et al. (1986) and Subrahmanya & Kapahi (1983), instead, proposed a non-evolving population of local ($z < 0.1$) low-luminosity radio galaxies as an explanation for the sub-mJy counts.

Optical identifications for a few samples show that $\sim (20$ – $30)\%$ of the radio sources in the sub-mJy regime are identified with optical counter-

parts brighter than $m_B \leq 22.0$, while $\sim 50\%$ are identified in deeper CCD frames reaching $m_B \sim 24.0\text{--}25.0$. These analyses show that the majority of the identified radio sources at the sub-mJy level are faint blue galaxies (Kron, Koo & Windhorst 1985; Windhorst et al. 1985, 1987, 1995; Thuan & Condon 1987), often showing peculiar optical morphology indicative of interacting, starburst or merging galaxies (Kron, Koo & Windhorst 1985; Windhorst, Dressler & Koo 1987) and seem to occur preferentially in pairs or small groups (Windhorst et al. 1995). This result is confirmed by the largest spectroscopic work so far available (Benn et al. 1993), which has proved that most of the optical counterparts with $m_B \lesssim 22.0$ of the sub-mJy sources have spectra similar to those of star-forming IRAS galaxies. Note, however, that the Benn et al. sample of spectroscopic identifications, although relatively large (58 redshifts), corresponds to a small fraction (slightly more than 10%) of the total number of radio sources in their sample.

The aim of this paper is to investigate the weak radio source population in an area of the sky, the *Marano Field*, which has been deeply surveyed in the optical and X-ray (ROSAT) bands. In this field a deep ROSAT observation (~ 60 ksec) has recently been carried out. About fifty X-ray sources have been detected in the inner $15'$ radius circle at a flux limit of $\sim 4 \times 10^{-15}$ erg cm $^{-2}$ s $^{-1}$ (Zamorani et al. in preparation). This inner part of the ROSAT field has been almost entirely covered by CCD exposures, in the U, B, V and R bands, taken with the ESO NTT, while a larger area ($\sim 1^\circ$ diameter) has been covered by ESO 3.6-m plates in the U, J and F bands. These optical data have been used to select a sample of ~ 70 spectroscopically confirmed quasars with $J \leq 22.5$. Fifty-two of these quasars constitute a complete sample with $J \leq 22.0$ (the MZZ sample, see Zitelli et al. 1992). The radio properties of this sample of quasars will be discussed in a future paper (Gruppioni et al., in preparation).

We observed this field at 1.4 and 2.4 GHz with the Australia Telescope Compact Array (ATCA). In this paper we present two samples of sources, complete at the $5\sigma_{local}$ level, corresponding to ~ 0.2 mJy at each frequency, extracted from an area of ~ 0.36 sq. deg. Our goals are (a) to measure the 1.4 and 2.4 GHz counts down to ~ 0.2 mJy and to compare them with the existing counts at similar frequencies (Windhorst et al. 1985, 1987 at 1.4 GHz; Condon 1984; Wall & Peacock 1985 at 2.7 GHz); (b) to determine the two point spectral index distribution of these sources and to study it for different flux density intervals for both the 1.4 and 2.4 GHz selected samples.

Radio observations, data reduction and the radio catalogues are described in §2. In §3 we present the 1.4 and 2.4 GHz counts. In §4 we discuss the spectral index distribution for different flux density intervals. Our conclusions are given in §5.

2 THE RADIO OBSERVATIONS

2.1 The ATCA Observations

The radio observations were carried out on 1994 January 4, 5, 6 and 7. They were made with the Australia Telescope Compact Array (ATCA) simultaneously at two different frequencies: 1.380 and 2.378 GHz (referred to as 1.4 and 2.4 GHz in the rest of the paper). In order to obtain a good coverage of the inner region of the ROSAT field ($\sim 20'$ radius) within the FWHM of the primary beam ($33'$ at 1.4 GHz and $22'$ at 2.4 GHz), a mosaicing pattern of four separate observations with different pointing positions was utilized. The four observations (12 hours each) were pointed at the vertices of a square with a side of 16 arcmin centered at the position of the Marano Field center ($\alpha(2000) = 03^h 15^m 09^s$, $\delta(2000) = -55^\circ 13' 57''$). The observing bandwidth was 128 MHz, consisting of 32×4 MHz channels. The primary flux density calibrator was PKS B1934–638, which was assumed to have flux densities of 16.24 and 13.05 Jy respectively at 1.4 and 2.4 GHz. As a phase and secondary amplitude calibrator the source PKS B0302–623 was used.

2.2 Data Reduction

The data were calibrated and reduced using the ATCA reduction package MIRIAD (Multi-channel Image Reconstruction Image Analysis and Display). First, each pointing was calibrated and reduced separately as a standard 12 hour exposure. After flagging of bad data and calibrating by using primary and secondary calibrators, the data were imaged utilizing the *multi-frequency synthesis* procedure available in MIRIAD. This procedure creates a single continuum image from a variety of frequencies. In this way the individual channels are gridded with their correct location in the u - v plane, rather than with some average location. Because of our large observing bandwidth (128 MHz), the *multi-frequency synthesis* technique was necessary, since it allowed us to reduce the bandwidth smearing and to obtain a better u - v coverage in a better beam. For each of the four single fields a 2048×2048 pixel image was constructed, with a pixel-size of 2.2×2.2 arcsec.

In order to reduce an interference which looked like a DC-offset and affected significantly our 1.4 GHz data, we were forced to restrict the usable band, using data only from channel 12 to channel 27, thus increasing the limiting flux at this frequency by about 40%. Moreover, the bandwidth restriction caused the reference frequency to be 1.370 GHz instead of the nominal 1.380 GHz.

For each frequency the four dirty maps were CLEANed separately. The source components were then restored by convolving them with a beam of $14''.5 \times 9''.5$ (FWHM), p.a. 15° and $9''.8 \times 5''.0$, p.a. 13° respectively for the 1.4 and 2.4 GHz maps. The final maps at the two frequen-

cies were then obtained by combining the four single maps using the mosaic procedure available in MIRIAD.

The minimum rms noise obtained in the central area of the field and in areas far from bright sources was comparable to the expected one, but the final noise resulted somewhat structured and irregularly distributed at low signal-to-noise ratio levels, especially in the 1.4 GHz map. In order to select a sample above a given threshold, defined in terms of *local* signal-to-noise ratio, a detailed analysis of the spatial rms noise distribution in the images was necessary.

We were then forced to construct and study in detail the rms noise map. To do this we utilized the NOAO reduction package IRAF (Image Reduction and Analysis Facility). The adopted procedure started with the creation of a *background* image, obtained by fitting every line of the map with a continuous function and clipping out every pixel with an absolute value greater than a fixed number of times the median value. The clipped pixels were substituted with their corresponding median value. We then computed a running mean of the *background* map and subtracted this mean from the *background* to obtain the residual image, from which the pixel by pixel rms noise map was finally derived.

The area from which we have extracted the complete samples of sources described in the next sub-Section is $36' \times 36'$. Outside this area the beam attenuation increases significantly the limiting flux at both frequencies.

Figure 1 shows the integral distributions of the percentage of pixels with a given rms noise as a function of rms noise for the two maps. The steeper curve for the 2.4 GHz map corresponds to the fact that the noise is significantly more uniform at this frequency: 95% of the pixels have an rms value in the range 40–150 μJy at 1.4 GHz and in the range 45–100 μJy at 2.4 GHz. These rms integral distributions have been used to compute the *visibility areas* as a function of flux which are necessary in order to properly derive the source counts (see Section 3).

2.3 The 1.4 GHz and 2.4 GHz Samples

At both frequencies we decided to select all sources whose peak flux density is greater than or equal to 5 times the local noise. Operatively, this was done by dividing the original map by the rms noise map described in Section 2.2 above and considering as real sources all the objects showing a signal-to-noise ratio greater than or equal to 5.

The $36' \times 36'$ area corresponds to about 4.5×10^4 and 1.2×10^5 beams at 1.4 and 2.4 GHz respectively. If the noise had been well behaved and gaussian distributed we would have expected less than one spurious source above $5\sigma_{local}$ at each frequency. Since this is not the case, in order to have an estimate of the number of the possibly spuri-

ous sources we checked for the presence of negative peaks with absolute value greater than $5\sigma_{local}$. Indeed, a few such peaks are present in the two maps, but all of them are found in the vicinity of the strongest and extended radio sources, probably due to unusually deep negative sidelobes, which are difficult to clean completely. Thus we are confident that at most one or two spurious sources are present in the samples.

The source parameters were derived by least-square fitting of the source surface brightness distribution using an extended two-dimensional Gaussian. The parameters derived by the fit are the source position, the peak and total fluxes (S_p and S_t), the Gaussian half-width and the position angle (deconvolved with the half-power width of the beam). For a few faint sources, by comparing the values of each pixel in the data with the corresponding best fitted values, we found that the Gaussian fitting algorithm produced a significant overestimate of the peak flux (see Condon 1996 for an extensive discussion about errors in Gaussian fits). For these sources we derived the peak flux by a second degree interpolation and the total flux by integrating the map values in a rectangle around the sources.

Tables 1 and 2 contain the data for the complete samples at 1.4 and 2.4 GHz, respectively. The Tables are arranged as follows:

Column (1) gives the source number (in right ascension order). For double or multiple sources (clearly resolved into two or more components) the components are labeled "A", "B", etc., followed by a line in which parameters for the total source are given. In a few cases single components in multiple sources below the completeness limit of the samples are also listed and are marked with an asterisk. *Columns (2) and (3)* give the right ascension and declination of each single component for equinox 2000. For multiple sources the positions have been computed as the flux weighted average position for all the components. *Columns (4) and (5)* give the peak and total flux density, each with its error (in mJy). *Columns (6) and (7)* give the deconvolved largest angular size (in arcsec) and the source position angle (in degrees) for resolved sources. *Column (8)* gives the peak signal-to-noise ratio.

By comparing the positions and the position angles of the sources detected at both frequencies we found that the average error in both right ascension and declination is ~ 0.7 arcsec and the average error in position angle is ~ 15 degrees. Both these errors are significantly larger than the formal errors produced by the fit. For this reason the formal errors for these parameters are not given in the Tables. In addition to these statistical errors, there appears to be a systematic difference of ~ 0.5 arcsec in right ascension between the 1.4 and 2.4 GHz maps, the origin of which is not understood.

The 1.4 and 2.4 GHz complete samples contain 63 and 48 sources respectively. Forty-three sources

are in common to the two samples; 9 of the 20 sources which are part of the 1.4 GHz complete sample only are detected at 2.4 GHz above $3\sigma_{local}$, while 3 of the 5 sources which are part of the 2.4 GHz complete sample only are detected at 1.4 GHz at the same σ_{local} level.

There are a few borderline cases in which it is not easy to distinguish between a close pair of unrelated sources and one source composed of several components. In Tables 1 and 2 there are six sources which we have considered double or multiple in either the 1.4 GHz or in the 2.4 GHz map or in both. Three of these sources have an angular distance (d) between different components smaller than 15 arcsec, while the other three have $15 < d < 25$ arcsec. The number of expected random pairs of unrelated sources with $d \lesssim 25$ arcsec, computed on the basis of the observed surface density in our fields, is about 1 or 2. Actually, there are two other pairs of 5σ components which are at about 25 arcsec from each other, namely sources 21 and 20, and 19 and 16 (at 1.4 GHz). They have not been considered to be different components of the same source mainly because of the large ratio between the fluxes of the two components (sources 16 and 19) or of their very flat spectral indices (sources 20 and 21), not consistent with the typical spectral indices of lobes in double radio sources. Figure 2 shows contour maps for the 6 sources classified as double or multiple in our samples.

In panel (a) 1.4 and 2.4 GHz maps are shown for two sources. Source 14(1.4 GHz)–9(2.4 GHz) presents the largest difference between the positions found for its components at 1.4 and 2.4 GHz. In particular, the position of component B at 1.4 GHz is displaced by ~ 4 arcsec to the north with respect to that at 2.4 GHz. This may be due to the fact that at higher frequency the emission peak could be associated to a flat spectrum "hot spot", while at lower frequency it is associated to the center of the lobe. Source 38(1.4 GHz)–30(2.4 GHz) is a classical triple source at lower frequency, while is a compact single source at higher frequency since only the core is detected above 5σ . In panel (b) 2.4 GHz maps are shown for the other four double or multiple sources. Source 10 is the radio source with the higher flux ($S_{1.4GHz} = 158$ mJy) in our sample and is identified with the quasar # 5571 of the MZZ sample. Source 22 is a multiple source with component B probably corresponding to the nucleus, since it has a flatter spectral index and its position coincides with that of a red point-like optical object. Sources 29 and 37 are classical double sources.

3 THE SOURCE COUNTS

The complete samples of sources with $S_p \geq 5\sigma_{local}$ at 1.4 and 2.4 GHz were used for the construction

of the source counts. Complex sources or sources with multiple components were treated as a single radio source. Every source was weighted for the reciprocal of its visibility area (fig. 1), that is the area over which the source could have been seen above the adopted limit of $5\sigma_{local}$ (Katgert et al. 1973). Figure 3 shows the ratio between the total and the peak flux as a function of flux for all the single component sources at 1.4 GHz. For most of the sources such a ratio is approximately normally distributed around 1, as expected for unresolved sources. The 1σ dispersion of the distribution is $\sim \pm 10\%$ for $S \gtrsim 1$ mJy and increases slightly at lower fluxes. The band indicated by the dashed curves in figure 3 contains the sources which we have considered to be unresolved. For these sources we have adopted the peak flux in computing the source counts, while for all the others, i.e. single component sources with S_t/S_p lying above the band drawn in figure 3, and sources clearly resolved into two or more components, we have adopted the total flux.

In Tables 3a and 3b the resulting 1.4 GHz and 2.4 GHz source counts are presented. The columns give the adopted flux density intervals, the average flux density in each interval, computed as the geometric mean of the two flux limits, the observed number of sources in each flux interval, the differential source density (in $\text{sr}^{-1} \text{Jy}^{-1}$), the normalized differential counts $nS^{2.5}$ (in $\text{sr}^{-1} \text{Jy}^{1.5}$) with estimated errors (as $n^{1/2}S^{2.5}$) and the integral counts (in sr^{-1}). In each table we do not report the data for the flux intervals (one at 1.4 GHz and two at 2.4 GHz) which contain only one source.

The 1.4 and 2.4 GHz normalized differential counts are plotted in figure 4a and 4b. In panel a) the solid curve represents the global fit to the counts obtained by Windhorst, Mathis & Neuschauer (1990) by fitting the counts from several 1.4 GHz surveys, while in panel b) our counts are compared with the 2.7 GHz counts derived by Condon (1984), on the basis of data by Wall, Pearson & Longair (1981) and with a prediction based on fluctuation analysis down to ~ 2 mJy obtained by Wall & Cooke (1975). Because of the slightly different frequencies our 2.4 GHz counts have been statistically transformed to 2.7 GHz with an effective spectral index $\alpha = +0.53$, equal to the median value found for the 2.4 GHz selected sample (see Section 4.2). Note that at this frequency our counts are the deepest available, since the flux density limit of Wall et al. (1981) is ~ 0.1 Jy and the curve from Condon (1984) is only an extrapolation at low flux densities based on steep spectrum and flat spectrum sources evolution models from Wall, Pearson & Longair (1981).

Our counts at both frequencies are in good agreement with the previous data. By transforming our 2.4 GHz data to 1.4 GHz with an effective spectral index equal to the median value found for the 2.4 GHz selected sample, we find

that also the source counts at this frequency are consistent with the curve from Windhorst, Mathis & Neuschauer (1990), although they are not sufficiently deep to show the well-known flattening observed in the counts at frequencies both above and below 2.4 GHz (see Wall 1994 for a recent discussion of counts at several frequencies).

A Maximum Likelihood fit to our 1.4 GHz counts with two power laws:

$$\frac{dN}{dS} \propto \begin{cases} S^{-\alpha_1} & \text{if } S > S_b \\ S^{-\alpha_2} & \text{if } S < S_b \end{cases}$$

gives the following best fit parameters: $\alpha_1 = 1.60 \pm 0.15$, $\alpha_2 = 2.15 \pm 0.40$, $S_b \sim 0.9$ mJy. Although the errors, which represent the projection on the α_1 and α_2 axes of the 1σ combined errors on the two slopes, are relatively large, our best fit parameters suggest that the re-steepening of the integral counts toward an Euclidean slope starts just below ~ 1 mJy, in agreement with Windhorst, van Heerde & Katgert (1984) and Condon & Mitchell (1984), while Windhorst et al. (1985, 1990), by fitting the counts to several 1.4 GHz survey, found that the change in slope starts around 5 mJy.

4 THE SPECTRAL INDEX DISTRIBUTION

As noted before (section 2.4), 20 of the 63 sources in the 1.4 GHz sample were not detected at 2.4 GHz at the $5\sigma_{local}$ level and 5 of the 48 sources in the 2.4 GHz sample were not detected at 1.4 GHz at the same level. For these sources we inspected our maps for detection at lower statistical level, and actually about half of them were detected at the $3\sigma_{local}$ level. For these sources we used their integrated flux to compute the spectral index and adopted the local rms noise as the flux density error; for the others, which remained undetected even at the $3\sigma_{local}$ level, we computed a limit on the spectral index, by assuming that their flux density was below the $3\sigma_{local}$ threshold level.

Since the maps at the two frequencies have two different beams, the fluxes given in Tables 1 and 2 do not allow a direct flux density comparison. Therefore, we computed the spectral indices (α ; $S \propto \nu^{-\alpha}$) for each source by using, for the 2.4 GHz sources, the integrated flux density obtained after convolving the 2.4 GHz image with the same beam width as the 1.4 GHz image ($14''.5 \times 9''.5$). For each spectral index we computed the corresponding error as :

$$\sigma_\alpha = \frac{\sqrt{(\sigma_{S_1}/S_1)^2 + (\sigma_{S_2}/S_2)^2}}{\ln(\nu_1) - \ln(\nu_2)}.$$

The data on the spectral indices are given in Table 4 for all the sources in the two complete samples. *Columns (1) and (2)* give the source numbers

in the 1.4 and 2.4 GHz catalogues, respectively; if a source is not in one of the complete samples no number is reported at that frequency. *Columns (3) and (4)* give the 1.4 and 2.4 GHz total flux densities and corresponding 1σ errors (in mJy). Sources which have a listed flux in this table and not in Tables 1 and 2 have $3\sigma_{local} < S_p < 5\sigma_{local}$. *Column (5)* gives the spectral index (or a limit on it) and its 1σ error.

Figures 5a and 5b show the spectral indices of the sources in the complete samples at 1.4 and 2.4 GHz, respectively, as a function of flux. Although qualitatively similar, the two distributions show some differences:

a) As expected, the median spectral indices (α_{med}) for the 2.4 GHz sample are smaller than the 1.4 GHz ones, because the higher frequency favours the detection of a higher fraction of flat spectrum sources. For both samples α_{med} has been computed using the ASURV package, which implements the methods described in Feigelson and Nelson (1985) and Isobe, Feigelson and Nelson (1986) to statistically analyze data with upper or lower limits. The resulting values for α_{med} are 0.81 ± 0.10 for the 1.4 GHz sample and 0.53 ± 0.08 for the 2.4 GHz sample.

b) If each sample is divided into two about equally populated subsamples, we find that the values for α_{med} at 1.4 GHz are consistent with being constant for the high and low flux subsamples (see the $\pm 1\sigma$ ranges for α_{med} in Figure 5a). This is in agreement with the results of Donnelly, Partridge & Windhorst (1987), who found that the median spectral index for their 1.46 GHz complete sample is approximately constant at ~ 0.75 in the whole range $0.25 \leq S_{1.46} \leq 100$ mJy. Viceversa, we have some indications, at $\sim 95\%$ confidence level, that the spectra for the 2.4 GHz sample flatten at lower fluxes (see Figure 5b). The values of α_{med} derived for fluxes greater than and less than 0.8 mJy at this frequency are 0.67 ± 0.09 and 0.38 ± 0.11 .

c) At both frequencies α_{med} is larger than the average α because of an asymmetry in the α distribution due to the presence of a non negligible number of objects with very flat or even inverted spectra. In particular, objects with inverted spectra, which appear at both frequencies for $S \lesssim 2$ mJy, constitute $\sim 13\%$ of the total 1.4 GHz sample and $\sim 25\%$ of the total 2.4 GHz. For this sample this percentage increases to $\sim 40\%$ for $S < 0.6$ mJy. These percentages are in good agreement with those found by Donnelly, Partridge & Windhorst (1987) at about the same flux limit: sources with inverted spectrum constitute $\sim 27\%$ and $\sim 8\%$ of their complete samples, respectively at 5 and 1.4 GHz. The tendency of an increasing percentage of sources with inverted spectra at even lower fluxes is suggested also by the recent result of Hammer et al. (1995), who find that about 50% of their optically identified μ Jy radio sources ($S_{4.86GHz} > 16 \mu$ Jy) do have inverted radio spec-

tra. Such sources in their sample are mainly identified with early-type galaxies at $z > 0.75$, with a smaller percentage of blue, emission-line galaxies at lower redshifts. On the basis of the inverted spectral indices, the authors conclude that for both classes of objects the radio emission is powered by a mini-AGN rather than by starburst activity. All the early-type galaxies with inverted spectrum in the Hammer et al. sample have very faint V magnitude, in the range $23 \lesssim V \lesssim 26$. Similar objects in the existing sub-mJy samples would have not been spectroscopically identified. To verify whether the objects with inverted spectrum in our sample are the "bright" counterparts of the objects found in the μ Jy sample, we are obtaining deep spectroscopic observations at the ESO 3.6-m telescope (Gruppioni et al., in preparation). On the basis of preliminary data for about 40% of our complete samples of radio sources, we indeed find that almost all of the spectroscopically observed sources with inverted radio spectrum are identified with early-type galaxies at intermediate redshift. Enhanced starburst activity, while present in a few sources with steep radio spectral index ($\alpha > 0.5$), is not seen in any of the optical counterparts of sources with inverted radio spectrum.

5 CONCLUSIONS

In this paper we have presented the first deep survey obtained at two frequencies (1.4 and 2.4 GHz) with the ATCA. With the use of a mosaic technique (four separate observations with different pointing positions) we have been able to obtain a reasonably low $5\sigma_{local}$ limiting flux over an area large enough (~ 0.36 sq. deg.) to provide acceptable statistics at each frequency. The complete samples of $5\sigma_{local}$ sources are constituted by 63 and 48 sources at 1.4 and 2.4 GHz respectively.

The main results of our analysis of the radio data are:

i) Our normalized differential counts at 1.4 GHz show a flattening below about one mJy, in agreement with the results from other 1.4 GHz deep surveys (Condon & Mitchell 1984; Condon 1984; Windhorst 1984; Windhorst et al. 1985). A formal Maximum Likelihood fit to our counts suggests a resteeptening toward an Euclidean slope, although with a relatively large error ($\alpha = 2.15 \pm 0.40$), just below ~ 1 mJy.

ii) Our 2.4 GHz counts are the deepest at this or similar frequencies (i.e. 2.7 GHz). They agree with previous counts at significantly higher flux (Wall, Pearson & Longair 1981; Condon 1984; Wall & Peacock 1985). Although no change in slope is seen in the 2.4 GHz counts, they are however consistent with the best fit curve at lower frequency.

iii) Dividing each sample into two about equally populated subsamples, we find that the

values for α_{med} at 1.4 GHz are consistent with being constant for the high and low flux subsamples, in agreement with the results of Donnelly, Partridge & Windhorst (1987). Viceversa, we have some indications (significant at $\sim 2\sigma$ level) that at 2.4 GHz α_{med} decreases at lower fluxes. Note that, since in analysing the distributions of the spectral indices for the complete samples at each frequency we fully used also the information given by the presence of a few limits on α , these results should not be affected by the biases discussed in Donnelly, Partridge & Windhorst (1987).

iv) At both frequencies α_{med} is larger than the average α because of an asymmetry in the α distribution due to the presence of a non negligible number of objects with very flat or even inverted spectra. In particular, objects with inverted spectra, which appear at both frequencies for $S \lesssim 2$ mJy, constitute $\sim 13\%$ of the total 1.4 GHz sample and $\sim 25\%$ of the total 2.4 GHz one. For this sample this percentage increases to $\sim 40\%$ for $S < 0.6$ mJy. The tendency of an increasing percentage of sources with inverted spectra at even lower fluxes is confirmed by the recent result of Hammer et al. (1995), who find that about 50% of their optically identified μ Jy radio sources ($S_{4.86GHz} > 16\mu$ Jy) do have inverted radio spectra.

Optical identifications of our radiosources and, in particular, of our inverted-spectrum faint sources should help in better understanding the nature of this population of objects. The results of such work will be presented in a following paper (Gruppioni et al., in preparation), which is presently in progress.

6 ACKNOWLEDGEMENTS

This paper is based on observations collected at the Australia Telescope Compact Array (ATCA), which is operated by the CSIRO Australia Telescope National Facility. The authors thank Roberto Fanti for helpful suggestions and for a careful reading of the manuscript. This work has been partially financed by the Italian Space Agency (ASI) under the contract ASI-1995-RS-152.

REFERENCES

- Benn C.R., Rowan-Robinson M., McMahon R.G., Broadhurst T.J. & Lawrence A., 1993, MNRAS, 263, 98
- Condon J.J., 1984, ApJ, 287, 461
- Condon J.J., 1989, ApJ, 338, 13
- Condon J.J., 1996, NRAO preprint
- Condon J.J. & Mitchell K.J., 1984, AJ, 89, 610
- Donnelly R.H., Partridge R.B. & Windhorst R.A., 1987, ApJ, 321, 94
- Feigelson E.D. & Nelson P.I., 1985, ApJ, 293, 192

- Fomalont E.B., Windhorst R.A., Kristian J.A. & Kellerman K.I., 1991, *AJ*, 102, 1258
- Hammer F., Crampton D., Lilly S.J., Le Fèvre O. & Kenet T., 1995, *MNRAS*, 276, 1085
- Isobe T., Feigelson E.D. & Nelson P.I., 1986, *ApJ*, 306, 490
- Katgert P., Katgert–Merkelijn J.K., Le Poole R.S. & van der Laan H., 1973, *A&A*, 23, 171
- Kellerman K.I., Fomalont E.B., Weistrop D. & Wall J.V., 1986, in Swings J.P., ed., *Highlights of Astronomy Vol. 6*. Reidel, Dordrecht, p. 367
- Kron R.G., Koo D.C. & Windhorst R.A., 1985, *A&A*, 146, 38
- Oort M.J.A., 1987, PhD Thesis, Univ. Leiden
- Oort M.J.A. & Windhorst R.A., 1985, *A&A*, 145, 405
- Rowan–Robinson M., Benn C.R., Lawrence A., McMahon R.G. & Broadhurst T.J., 1993, *MNRAS*, 263, 123
- Subrahmanya C.R. & Kapahi V.K., 1983, in Abell G.O. & Chincarini G., eds, *Proc. of IAU Symp. 104, The Early Evolution of the Universe and its Present Structure*. Reidel, Dordrecht, p. 47
- Thuan T.X. & Condon J.J., 1987, *ApJL*, L9
- Wall J.V., 1994, *Aust.J.Phys.*, 47, 625
- Wall J.V. & Cooke D.J., 1975, *MNRAS*, 171, 9
- Wall J.V. & Peacock J.A., 1985, *MNRAS*, 216, 173
- Wall J.V., Pearson T.J. & Longair M.S., 1981, *MNRAS*, 196, 597.
- Wall J.V., Benn C.R., Grueff G. & Vigotti M., 1986, in Swings J.P., ed., *Highlights of Astronomy Vol. 7*. Reidel, Dordrecht, p. 345
- Windhorst R.A., 1984, PhD Thesis, Univ. Leiden
- Windhorst R.A., Dressler A. & Koo D.C., 1987, in Hewitt A., Burbidge G. & Fang L.Z., eds, *Observational Cosmology*. Reidel, Dordrecht, p. 573
- Windhorst R.A., Fomalont E.B., Kellermann K.I., Partridge R.B., Richards E., Franklin B.E., Pascarella S.M. & Griffiths R.E., 1995, *Nature*, 375, 471
- Windhorst R.A., Fomalont E.B., Partridge R.B. & Lowenthal J.D., 1993, *ApJ*, 405, 498
- Windhorst R.A., van Heerde G.M. & Katgert P., 1984, *A&AS*, 58, 1
- Windhorst R.A., Mathis D.F. & Neuschaefer L.W., 1990, in Kron R.G., ed., *ASP Conf. Ser. Vol. 10, Evolution of the Universe of Galaxies*. Bookcrafters, Provo, p. 389
- Windhorst R.A., Miley G.K., Owen F.N., Kron R.G. & Koo D.C., 1985, *ApJ*, 289, 494
- Zitelli V., Mignoli M., Zamorani G., Marano B. & Boyle B.J., 1992, *MNRAS*, 256, 349

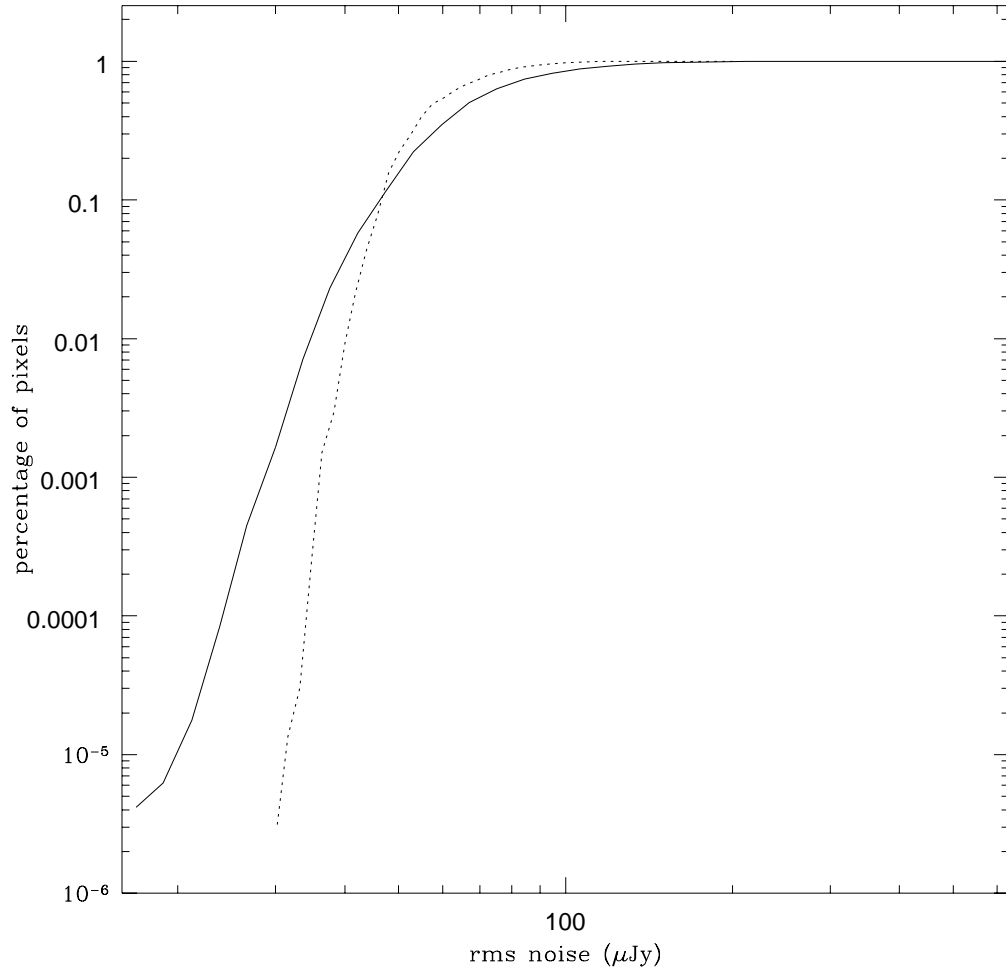
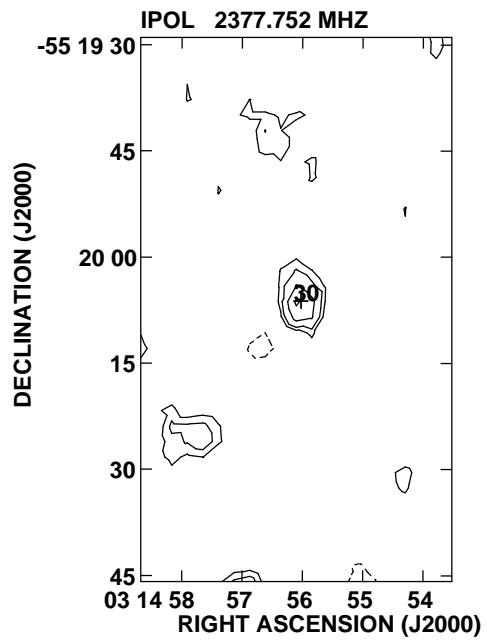
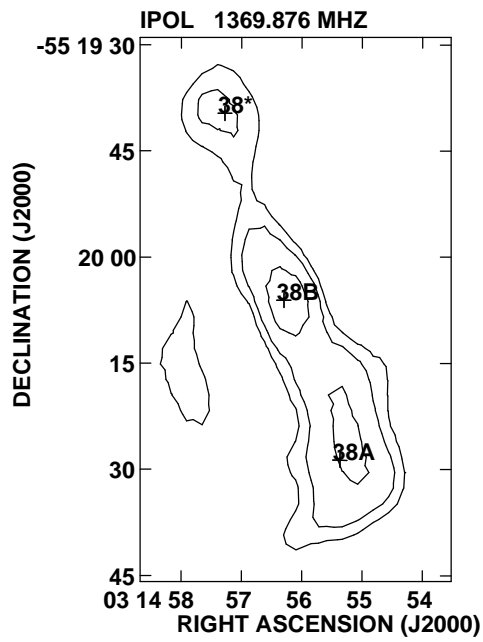
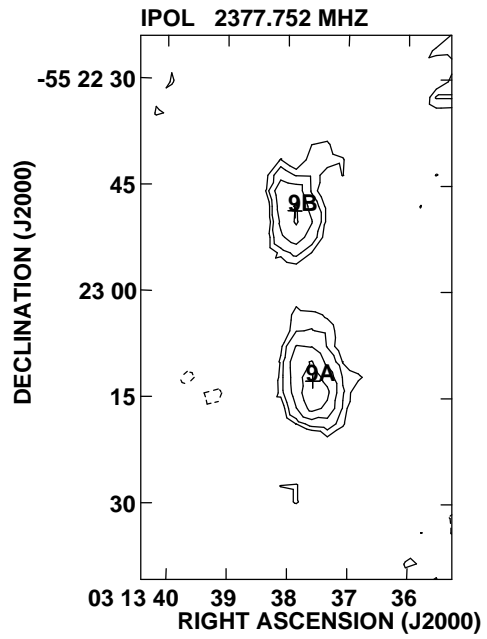
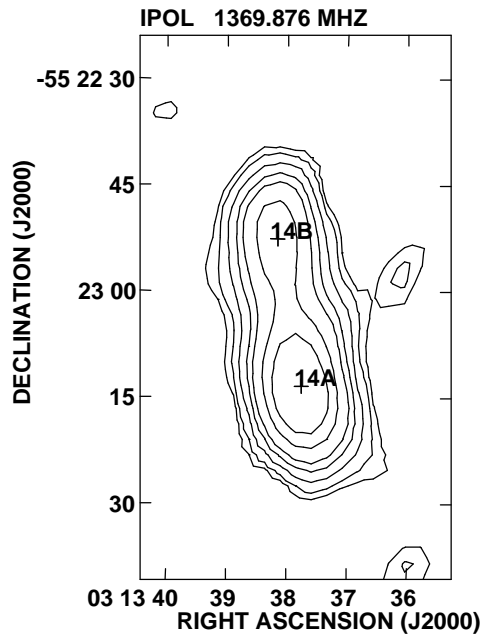


Figure 1: Integral distribution of the percentage of pixels with a given rms noise as a function of rms noise in the 1.4 (solid line) and 2.4 GHz (dotted line) map.



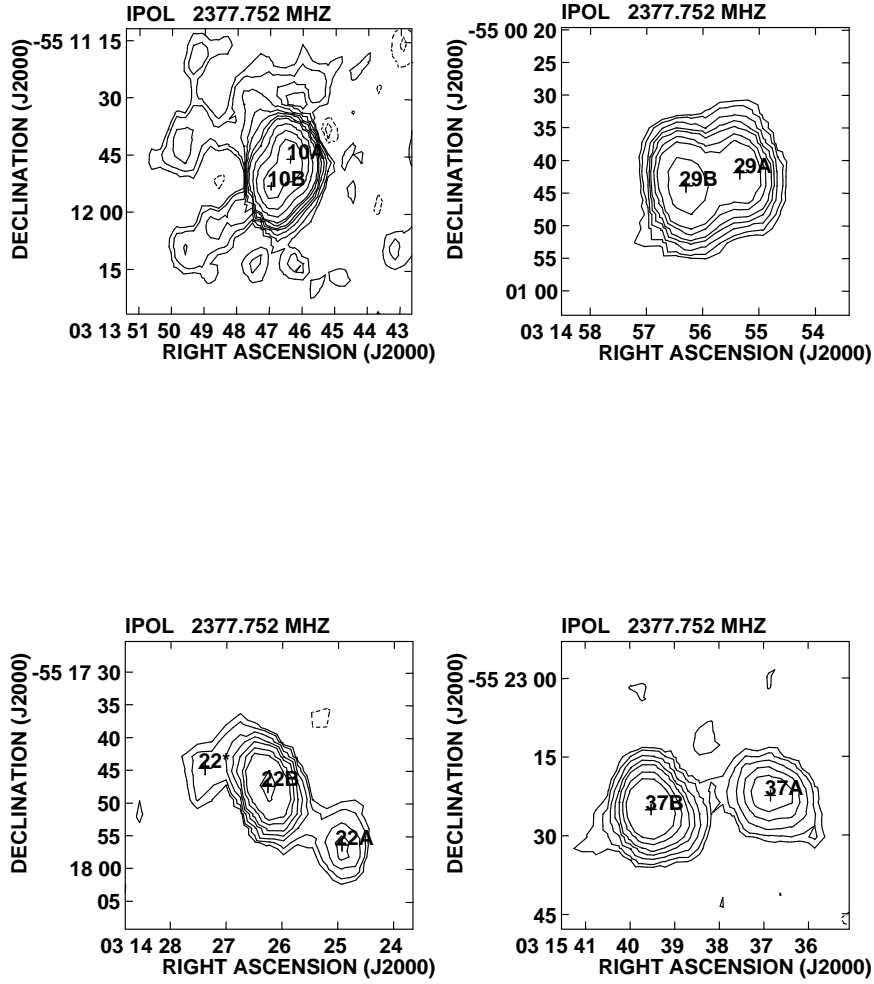


Figure 2: Contour diagrams of the six sources classified as double or multiple. The contour levels are at -5 , -3 (dashed), 2 , 3 , 5 , 7.5 , 10 , 15 , 20 , 40 , 60 , 80 , 160 times the σ_{local} for all the sources. In panel (a) 1.4 and 2.4 GHz maps are shown for two sources, while in panel (b) 2.4 GHz maps are shown for the other four double or multiple sources.

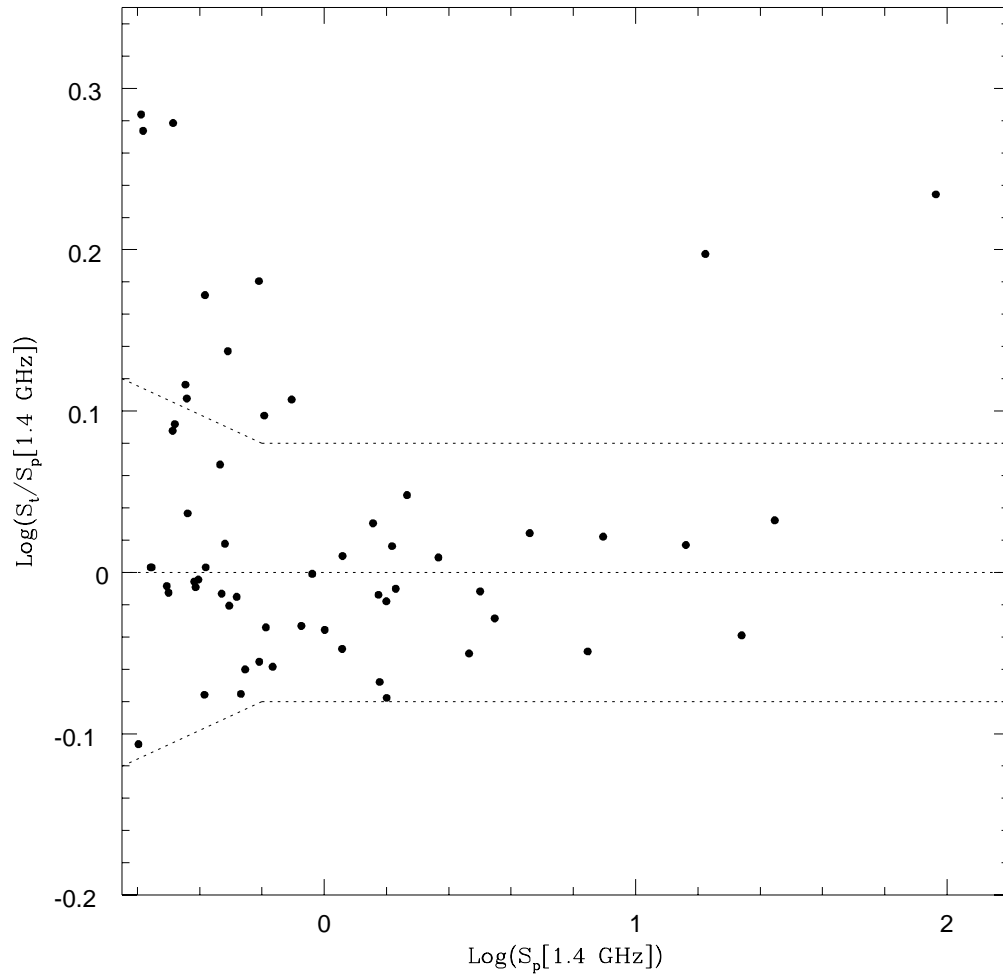


Figure 3: Total-to-peak flux ratio distribution as a function of peak flux for single component sources of the 1.4 GHz sample. The band defined by the dashed curve contains the sources which we have considered unresolved.

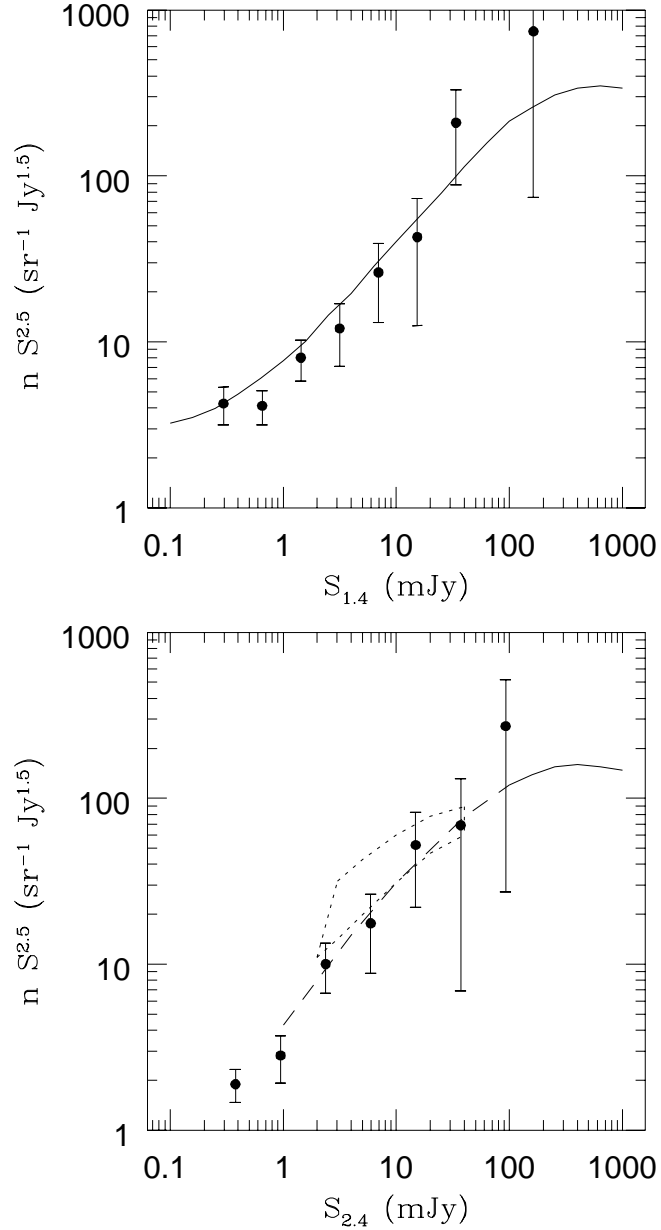


Figure 4: The normalized differential source counts. The abscissa gives the flux density (mJy) and the ordinate gives the differential number of sources normalized by $S^{2.5}$ ($\text{sr}^{-1} \text{Jy}^{+1.5}$). (a) The counts at 1.4 GHz. The solid line represents the global fit to the counts obtained by Windhorst, Mathis & Neuschauer (1990) by fitting the counts from 24 different 1.4 GHz surveys. (b) The counts at 2.4 GHz transformed to 2.7 GHz with an effective spectral index $\alpha=+0.53$. The solid line represents the fit obtained by Condon (1984) to the data from Wall, Pearson & Longair (1981), while the dashed line is a low flux extrapolation of the counts based on a source evolution model from Wall, Pearson & Longair. The dotted area represents the estimate of the source counts from a background deflection analysis from Wall & Cooke (1975).

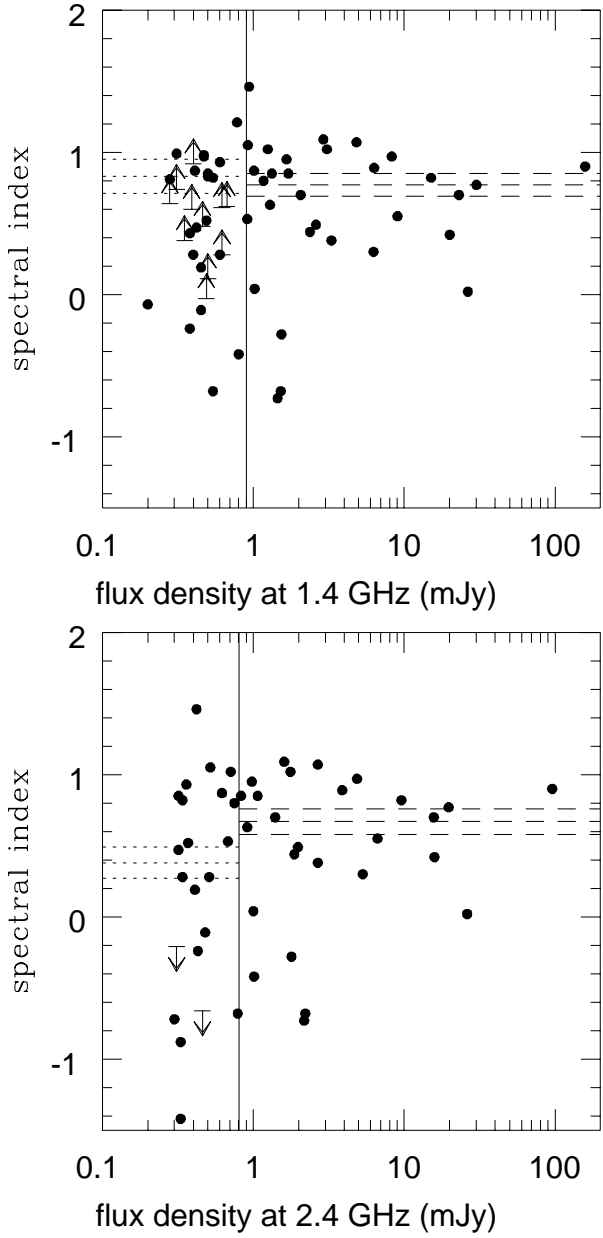


Figure 5: The spectral index as a function of flux density for sources in the 1.4 (a) and 2.4 GHz (b) complete samples. Each sample has been divided into two about equally populated subsamples (separated by the solid vertical line in figures), for which the median spectral index (α_{med}) and its 1σ error has been reported (dotted and dashed horizontal lines respectively for the low and high flux density subsamples). The arrows represents the upper and lower limits on α respectively in the 2.4 and 1.4 GHz complete samples.

TABLE 1: THE 1.4 GHz SAMPLE

Number	RA (2000)	DEC (2000)	S_P (mJy)	S_T (mJy)	Major Axis (arcsec)	P.A. (degrees)	S/N_{local}
01	03 13 08.90	-55 29 55.2	7.87 ± 0.05	8.28 ± 0.14	< 4.9		98.3
02	03 13 10.25	-55 15 11.2	0.33 ± 0.07	0.62 ± 0.13	14.0	35.6	5.0
03	03 13 13.33	-55 01 58.8	16.76 ± 0.20	26.40 ± 0.64	9.6	130.7	15.3
04	03 13 17.88	-55 14 59.7	0.49 ± 0.04	0.67 ± 0.13	11.1	31.0	5.3
05	03 13 18.23	-55 13 07.4	0.62 ± 0.05	0.54 ± 0.15	< 8.4		7.5
06	03 13 19.17	-55 27 09.5	0.84 ± 0.04	0.78 ± 0.10	< 7.5		11.6
07	03 13 19.30	-55 11 39.5	0.64 ± 0.09	0.80 ± 0.09	< 20.8		7.6
08	03 13 19.41	-55 16 17.4	0.39 ± 0.07	0.39 ± 0.07	< 16.4		5.6
09	03 13 22.02	-55 13 51.1	1.58 ± 0.04	1.52 ± 0.11	< 4.8		20.3
10	03 13 23.15	-55 18 40.8	21.91 ± 0.19	20.02 ± 0.61	< 3.9		134.9
11	03 13 30.65	-55 24 31.3	0.26 ± 0.03	0.49 ± 0.10	16.2	27.5	5.2
12	03 13 32.92	-55 17 34.1	0.48 ± 0.05	0.50 ± 0.05	< 9.6		7.6
13	03 13 33.65	-55 30 44.5	0.68 ± 0.09	0.60 ± 0.17	< 7.5		8.0
14A	03 13 37.76	-55 23 13.4	1.30 ± 0.03	1.81 ± 0.07	11.2	4.3	24.2
14B	03 13 38.16	-55 22 52.6	0.85 ± 0.03	0.99 ± 0.09	8.9	164.0	15.8
14	03 13 37.85	-55 23 06.0		2.91 ± 0.12			
15	03 13 46.66	-55 11 48.6	92.20 ± 0.62	158.00 ± 2.00	12.3	147.7	801.7
16	03 13 51.74	-55 08 16.7	1.59 ± 0.07	1.33 ± 0.23	< 11.1		19.2
17	03 13 51.80	-54 58 58.0	3.17 ± 0.04	3.08 ± 0.13	< 4.4		54.6
18	03 13 52.12	-55 21 14.6	0.28 ± 0.03	0.28 ± 0.09	< 11.0		5.4
19	03 13 54.36	-55 08 08.4	7.02 ± 0.09	6.27 ± 0.28	< 5.0		85.1
20	03 13 54.91	-55 01 13.1	0.39 ± 0.07	0.38 ± 0.07	< 13.2		5.9
21	03 13 54.96	-55 00 48.3	1.14 ± 0.04	1.02 ± 0.11	< 7.8		18.8
22	03 13 56.99	-55 23 17.5	0.50 ± 0.06	0.47 ± 0.06	< 9.4		7.9
23	03 14 06.85	-55 30 54.7	0.33 ± 0.06	0.40 ± 0.10	< 12.8		5.7
24	03 14 07.42	-55 04 58.1	0.36 ± 0.05	0.46 ± 0.15	< 18.2		6.0
25	03 14 15.54	-55 05 34.9	3.53 ± 0.05	3.30 ± 0.17	< 4.8		49.6
26	03 14 17.01	-55 27 07.1	0.54 ± 0.06	0.45 ± 0.06	< 10.3		9.7
27	03 14 19.20	-54 56 46.2	2.92 ± 0.05	2.60 ± 0.14	< 4.6		47.1
28	03 14 23.49	-55 30 23.9	1.70 ± 0.04	1.66 ± 0.13	< 6.6		24.9
29	03 14 24.06	-54 57 01.2	0.41 ± 0.03	0.62 ± 0.10	12.3	28.6	7.4
30A	03 14 25.16	-55 17 56.8	1.18 ± 0.02	1.18 ± 0.07	< 5.9		16.5
30B	03 14 26.40	-55 17 47.6	4.19 ± 0.03	4.27 ± 0.08	< 3.8		58.7
30C	03 14 27.28	-55 17 47.5	0.74 ± 0.03	1.20 ± 0.08	< 14.7		10.4
30	03 14 26.34	-55 17 49.2		6.32 ± 0.10			
31	03 14 34.33	-54 57 47.3	1.00 ± 0.04	0.92 ± 0.13	< 6.4		13.1
32	03 14 39.44	-55 18 59.4	0.52 ± 0.03	0.50 ± 0.11	< 8.5		8.6
33	03 14 44.76	-55 21 11.1	4.57 ± 0.03	4.83 ± 0.09	4.0	22.8	73.4
34	03 14 49.17	-55 09 12.3	0.36 ± 0.03	0.40 ± 0.09	< 8.0		6.9
35	03 14 51.30	-55 19 33.2	0.33 ± 0.05	0.41 ± 0.05	< 10.0		6.6
36	03 14 53.11	-55 07 27.6	1.15 ± 0.03	1.17 ± 0.08	< 6.3		21.3
37	03 14 55.25	-54 57 46.8	0.79 ± 0.04	1.01 ± 0.11	11.9	38.1	11.4
38A	03 14 55.37	-55 20 28.7	0.30 ± 0.02	0.71 ± 0.07	19.0	147.3	5.1
38B	03 14 56.30	-55 20 06.1	0.36 ± 0.03	0.57 ± 0.08	< 25.2		6.4
38*	03 14 57.28	-55 19 39.7	0.21 ± 0.02	0.28 ± 0.06	< 10.6		3.6
38	03 14 56.30	-55 20 06.1		1.25 ± 0.11			
39A	03 14 55.42	-55 00 42.1	8.37 ± 0.14	9.39 ± 0.41	5.1	157.4	74.6
39B	03 14 56.35	-55 00 43.9	13.98 ± 0.15	14.03 ± 0.42	< 4.3		126.4
39	03 14 56.00	-55 00 43.2		23.10 ± 0.59			
40	03 14 57.39	-55 09 41.3	0.65 ± 0.03	0.60 ± 0.09	< 7.0		13.6
41	03 15 10.06	-55 05 18.8	1.49 ± 0.03	1.45 ± 0.09	< 4.3		27.4
42	03 15 10.70	-55 25 58.5	27.96 ± 0.10	30.12 ± 0.29	3.6	97.0	277.8
43	03 15 18.23	-55 21 06.1	0.42 ± 0.06	0.42 ± 0.10	< 8.3		6.8
44	03 15 19.36	-54 59 43.7	14.51 ± 0.08	15.08 ± 0.24	3.2	25.6	184.2
45	03 15 22.06	-55 06 34.5	0.25 ± 0.05	0.20 ± 0.09	< 8.8		5.1
46	03 15 22.95	-55 09 15.4	0.26 ± 0.05	0.50 ± 0.07	22.2	6.7	5.7
47	03 15 32.66	-55 23 36.6	0.36 ± 0.06	0.47 ± 0.09	< 8.6		5.7
48	03 15 32.81	-55 11 28.3	0.46 ± 0.04	0.54 ± 0.13	< 12.7		10.0
49A	03 15 37.01	-55 23 22.8	1.51 ± 0.04	2.67 ± 0.13	11.2	96.3	26.0
49B	03 15 39.54	-55 23 24.7	4.87 ± 0.05	6.68 ± 0.14	7.1	102.3	84.0
49	03 15 38.82	-55 23 24.2		9.04 ± 0.19			

TABLE 1: CONTINUE

Number	RA (2000)	DEC (2000)	S_P (mJy)	S_T (mJy)	Major Axis (arcsec)	P.A. (degrees)	S/N_{local}
50	03 15 43.06	-55 20 21.6	0.28 ± 0.05	0.28 ± 0.05	< 11.3		5.5
51	03 15 49.42	-55 05 44.5	0.56 ± 0.03	0.49 ± 0.09	< 6.5		10.8
52	03 15 53.60	-55 13 53.3	1.84 ± 0.03	2.06 ± 0.09	5.3	28.1	33.4
53	03 15 54.47	-55 14 25.9	1.43 ± 0.03	1.54 ± 0.10	< 5.9		25.9
54	03 15 54.57	-55 02 02.8	0.92 ± 0.06	0.91 ± 0.18	< 9.5		15.0
55	03 16 06.00	-55 28 35.6	0.32 ± 0.05	0.31 ± 0.05	< 15.0		5.9
56	03 16 06.49	-55 30 40.7	2.33 ± 0.04	2.38 ± 0.13	< 5.0		33.0
57	03 16 10.27	-55 11 49.9	1.65 ± 0.03	1.71 ± 0.10	< 4.7		33.8
58	03 16 20.80	-55 30 18.4	1.51 ± 0.04	1.29 ± 0.12	< 7.0		24.3
59	03 16 41.73	-55 28 39.4	0.38 ± 0.07	0.38 ± 0.07	< 9.5		5.4
60	03 16 53.32	-55 17 08.00	0.62 ± 0.03	0.94 ± 0.08	12.4	29.2	10.8
61	03 17 05.78	-55 27 17.7	0.31 ± 0.06	0.31 ± 0.06	< 10.0		5.3
62	03 17 06.47	-55 19 49.2	0.47 ± 0.06	0.45 ± 0.06	< 10.8		7.3
63	03 17 13.14	-55 19 47.4	0.41 ± 0.04	0.35 ± 0.11	< 7.8		5.9

TABLE 2: THE 2.4 GHz SAMPLE

Number	RA (2000)	DEC (2000)	S_P (mJy)	S_T (mJy)	Major Axis (arcsec)	P.A. (degrees)	S/N_{local}
01	03 13 08.72	-55 29 54.9	5.01 ± 0.12	4.53 ± 0.39	< 3.5		41.4
02	03 13 13.32	-55 01 58.6	7.85 ± 0.13	27.08 ± 0.41	11.6	119.3	103.2
03	03 13 18.15	-55 13 05.8	0.80 ± 0.04	0.81 ± 0.15	< 5.7		8.6
04	03 13 19.21	-55 11 38.4	1.03 ± 0.04	1.20 ± 0.15	< 4.4		12.0
05	03 13 21.91	-55 13 51.1	2.26 ± 0.06	2.15 ± 0.20	< 3.9		27.6
06	03 13 22.56	-55 12 57.4	0.46 ± 0.09	0.55 ± 0.09	< 10.6		5.2
07	03 13 22.97	-55 18 40.2	14.97 ± 0.23	14.99 ± 0.74	< 2.7		193.7
08	03 13 33.33	-55 30 44.5	0.59 ± 0.05	0.47 ± 0.14	< 7.5		7.0
09A	03 13 37.58	-55 23 12.7	0.54 ± 0.03	0.85 ± 0.08	7.7	8.0	8.8
09B	03 13 37.89	-55 22 48.6	0.44 ± 0.03	0.62 ± 0.10	7.8	166.7	7.3
09	03 13 37.71	-55 23 02.6		1.58 ± 0.13			
10A	03 13 46.37	-55 11 45.9	37.83 ± 0.16	51.15 ± 0.52	4.9	8.1	356.6
10B	03 13 46.96	-55 11 52.9	27.22 ± 0.15	31.88 ± 0.47	2.7	105.5	256.7
10	03 13 46.60	-55 11 48.6		89.00 ± 0.70			
11	03 13 50.80	-55 05 55.5	0.29 ± 0.05	0.30 ± 0.05	< 7.6		5.4
12	03 13 51.78	-54 58 58.6	1.86 ± 0.04	1.78 ± 0.13	< 3.2		29.0
13	03 13 51.80	-55 08 17.0	0.95 ± 0.05	0.80 ± 0.16	< 4.5		15.5
14	03 13 54.34	-55 08 08.5	4.96 ± 0.06	5.46 ± 0.18	< 4.8		80.8
15	03 13 54.85	-55 01 12.3	0.51 ± 0.06	0.52 ± 0.06	< 4.7		10.1
16	03 13 54.97	-55 00 48.2	1.03 ± 0.03	1.11 ± 0.09	< 4.7		18.0
17	03 14 15.55	-55 05 34.7	2.69 ± 0.04	2.51 ± 0.13	< 2.5		49.0
18	03 14 16.14	-55 07 06.3	0.30 ± 0.05	0.31 ± 0.05	< 7.1		6.0
19	03 14 16.85	-55 27 06.6	0.50 ± 0.04	0.46 ± 0.12	< 5.7		8.0
20	03 14 19.22	-54 56 46.1	2.12 ± 0.04	2.17 ± 0.12	< 3.0		26.5
21	03 14 23.34	-55 30 23.5	1.19 ± 0.06	0.91 ± 0.18	< 6.0		14.9
22A	03 14 24.93	-55 17 56.3	0.60 ± 0.04	0.58 ± 0.13	< 5.5		9.6
22B	03 14 26.26	-55 17 47.4	3.24 ± 0.05	3.27 ± 0.15	< 3.7		51.8
22*	03 14 27.38	-55 17 44.7	0.31 ± 0.04	0.38 ± 0.11	< 8.3		4.8
22	03 14 26.26	-55 17 47.4		3.28 ± 0.23			
23	03 14 34.26	-54 57 48.6	0.50 ± 0.04	0.69 ± 0.13	9.5	22.9	7.0
24	03 14 39.33	-55 19 00.5	0.36 ± 0.03	0.30 ± 0.12	< 7.3		6.1
25	03 14 44.61	-55 21 10.8	2.69 ± 0.05	2.49 ± 0.15	< 4.4		50.2
26	03 14 49.02	-55 09 12.1	0.28 ± 0.03	0.31 ± 0.11	< 7.0		5.2
27	03 14 53.08	-55 07 27.8	0.60 ± 0.03	0.80 ± 0.08	5.0	11.1	10.8
28	03 14 55.18	-54 57 47.8	0.60 ± 0.08	0.66 ± 0.08	< 12.2		7.7
29A	03 14 55.34	-55 00 41.8	4.28 ± 0.05	5.69 ± 0.16	4.1	110.2	67.4
29B	03 14 56.30	-55 00 43.9	7.81 ± 0.05	9.91 ± 0.17	3.6	102.2	122.9
29	03 14 55.95	-55 00 43.13		16.09 ± 0.23			
30	03 14 56.03	-55 20 06.2	0.43 ± 0.04	0.44 ± 0.12	< 5.9		7.1
31	03 14 57.45	-55 09 41.5	0.33 ± 0.04	0.36 ± 0.12	< 7.0		5.6
32	03 15 10.02	-55 05 18.7	2.30 ± 0.04	2.28 ± 0.13	< 2.0		40.6
33	03 15 10.60	-55 25 58.3	16.99 ± 0.09	19.63 ± 0.30	2.9	68.9	201.4
34	03 15 18.23	-55 21 06.2	0.33 ± 0.05	0.38 ± 0.05	< 10.2		6.2
35	03 15 19.34	-54 59 43.5	8.33 ± 0.04	9.37 ± 0.14	2.6	158.1	127.0
36	03 15 32.97	-55 11 28.4	0.34 ± 0.03	0.40 ± 0.10	3.8	50.3	5.9
37A	03 15 36.85	-55 23 22.4	0.76 ± 0.03	2.01 ± 0.08	10.6	85.0	14.5
37B	03 15 39.53	-55 23 25.0	2.41 ± 0.03	5.02 ± 0.09	7.4	97.2	44.8
37	03 15 38.76	-55 23 24.3		6.40 ± 0.12			
38	03 15 49.49	-55 05 43.7	0.43 ± 0.05	0.44 ± 0.05	< 10.0		9.1
39	03 15 53.59	-55 13 53.2	1.31 ± 0.03	1.45 ± 0.10	3.1	8.8	22.7
40	03 15 54.47	-55 14 26.3	1.78 ± 0.03	1.86 ± 0.09	< 2.8		30.8
41	03 15 54.49	-55 02 03.2	0.73 ± 0.04	0.76 ± 0.12	< 6.6		13.4
42	03 16 06.49	-55 30 40.6	1.76 ± 0.04	2.05 ± 0.14	< 6.0		23.8
43	03 16 10.27	-55 11 49.6	1.09 ± 0.03	1.06 ± 0.10	< 3.2		19.7
44	03 16 20.78	-55 30 18.9	0.91 ± 0.04	0.87 ± 0.12	< 4.6		13.9
45	03 16 23.24	-55 04 09.9	0.28 ± 0.05	0.28 ± 0.05	< 12.7		5.7
46	03 16 53.27	-55 17 07.2	0.39 ± 0.06	0.41 ± 0.11	< 9.8		6.3
47	03 16 56.63	-55 24 53.0	0.35 ± 0.03	0.49 ± 0.11	< 10.6		5.4
48	03 17 06.51	-55 19 50.8	0.41 ± 0.05	0.39 ± 0.15	< 7.6		5.4

TABLE 3a: THE 1.4 GHZ RADIO SOURCE COUNTS

S	$\langle S \rangle$	N_s	dN/dS	$nS^{2.5}$	$N(> S)$
(mJy)	(mJy)		(sr ⁻¹ Jy ⁻¹)	(sr ⁻¹ Jy ^{1.5})	(sr ⁻¹)
0.20–0.44	0.30	15	2.80×10^9	4.2 ± 1.1	1.65×10^6
0.44–0.97	0.65	19	3.78×10^8	4.1 ± 0.9	4.61×10^5
0.97–2.13	1.44	13	1.03×10^8	8.0 ± 2.2	2.66×10^5
2.13–4.69	3.16	6	2.15×10^7	12.1 ± 4.9	1.46×10^5
4.69–10.3	6.95	4	6.51×10^6	26.2 ± 13.1	9.15×10^4
10.3–22.7	15.29	2	1.48×10^6	42.8 ± 30.2	5.49×10^4
22.7–49.9	33.63	3	1.01×10^6	209.3 ± 120.9	3.66×10^4

TABLE 3b: THE 2.4 GHZ RADIO SOURCE COUNTS

S	$\langle S \rangle$	N_s	dN/dS	$nS^{2.5}$	$N(> S)$
(mJy)	(mJy)		(sr ⁻¹ Jy ⁻¹)	(sr ⁻¹ Jy ^{1.5})	(sr ⁻¹)
0.22–0.55	0.35	19	7.09×10^8	1.6 ± 0.4	5.99×10^5
0.55–1.38	0.87	11	1.22×10^8	2.7 ± 0.8	2.65×10^5
1.38–3.44	2.17	9	3.99×10^7	8.8 ± 2.9	1.65×10^5
3.44–8.59	5.44	4	7.10×10^6	15.5 ± 7.7	8.24×10^4
8.59–21.5	13.59	3	2.13×10^6	45.8 ± 26.5	4.58×10^4

TABLE 4: THE 2.4–1.4 GHz SPECTRAL INDEX

Number		$S_{1.4}$	$S_{2.4}$	α
1.4 GHz	2.4 GHz	(mJy)	(mJy)	
01	01	8.28 ± 0.14	4.86 ± 0.15	0.97 ± 0.07
02		0.62 ± 0.13	< 0.53	> 0.28
03	02	26.40 ± 0.64	26.14 ± 0.50	0.02 ± 0.06
04		0.67 ± 0.13	< 0.48	> 0.62
05	03	0.54 ± 0.15	0.79 ± 0.12	-0.68 ± 0.57
06		0.78 ± 0.10	0.40 ± 0.13	1.21 ± 0.64
07	04	0.80 ± 0.09	1.01 ± 0.12	-0.42 ± 0.29
08		0.39 ± 0.07	< 0.28	> 0.60
09	05	1.52 ± 0.11	2.21 ± 0.17	-0.68 ± 0.19
	06	< 0.32	0.46 ± 0.09	< -0.66
10	07	20.02 ± 0.61	15.90 ± 0.11	0.42 ± 0.06
11		0.49 ± 0.10	< 0.50	> -0.03
12		0.50 ± 0.05	0.32 ± 0.07	0.83 ± 0.42
13	08	0.60 ± 0.17	0.51 ± 0.10	0.28 ± 0.64
14A	09A	1.81 ± 0.07	0.90 ± 0.09	1.27 ± 0.19
14B	09B	0.99 ± 0.09	0.68 ± 0.11	0.67 ± 0.33
14	09	2.91 ± 0.12	1.60 ± 0.14	1.09 ± 0.17
15	10	158.00 ± 0.74	95.94 ± 1.08	0.90 ± 0.02
	11	0.20 ± 0.05	0.30 ± 0.05	-0.72 ± 0.57
16	13	1.33 ± 0.23	0.83 ± 0.14	0.85 ± 0.44
17	12	3.08 ± 0.13	1.76 ± 0.13	1.02 ± 0.16
18		0.28 ± 0.05	< 0.20	> 0.64
19	14	6.27 ± 0.28	5.31 ± 0.17	0.30 ± 0.10
20	15	0.38 ± 0.06	0.43 ± 0.06	-0.24 ± 0.41
21	16	1.02 ± 0.11	1.00 ± 0.06	0.04 ± 0.22
22		0.47 ± 0.06	0.28 ± 0.06	0.97 ± 0.46
23		0.40 ± 0.10	< 0.24	> 0.92
24		0.46 ± 0.15	< 0.36	> 0.48
25	17	3.30 ± 0.17	2.68 ± 0.13	0.38 ± 0.13
	18	0.20 ± 0.07	0.33 ± 0.13	-0.88 ± 0.99
26	19	0.45 ± 0.06	0.48 ± 0.12	-0.11 ± 0.50
27	20	2.60 ± 0.14	1.98 ± 0.12	0.49 ± 0.15
28	21	1.66 ± 0.13	0.98 ± 0.15	0.95 ± 0.31
29		0.62 ± 0.10	< 0.44	> 0.61
30A	22A	1.18 ± 0.07	0.70 ± 0.12	0.94 ± 0.32
30B	22B	4.27 ± 0.08	3.20 ± 0.12	0.52 ± 0.08
30C	22*	1.20 ± 0.08	0.38 ± 0.11	1.43 ± 0.54
30	22	6.32 ± 0.10	3.88 ± 0.17	0.89 ± 0.08
31	23	0.92 ± 0.13	0.52 ± 0.12	1.05 ± 0.50
32	24	0.50 ± 0.11	0.32 ± 0.11	0.85 ± 0.75

TABLE 4: CONTINUE

Number		S _{1.4}	S _{2.4}	α
1.4 GHz	2.4 GHz	(mJy)	(mJy)	
33	25	4.83 ± 0.09	2.68 ± 0.15	1.07 ± 0.11
34	26	0.40 ± 0.09	0.34 ± 0.10	0.28 ± 0.69
35		0.41 ± 0.05	0.25 ± 0.06	0.87 ± 0.47
36	27	1.17 ± 0.08	0.75 ± 0.10	0.80 ± 0.27
37	28	1.01 ± 0.10	0.62 ± 0.08	0.87 ± 0.31
38A		0.71 ± 0.07	< 0.58	> 0.36
38B	30	0.57 ± 0.08	0.42 ± 0.12	0.53 ± 0.58
38*		0.28 ± 0.06	< 0.24	> 0.28
38	30	1.25 ± 0.11	0.71 ± 0.14	1.02 ± 0.40
39A	29A	9.39 ± 0.41	5.66 ± 0.14	0.92 ± 0.09
39B	29B	14.03 ± 0.42	9.94 ± 0.16	0.63 ± 0.06
39	29	23.10 ± 0.59	15.70 ± 0.19	0.70 ± 0.05
40	31	0.60 ± 0.09	0.36 ± 0.16	0.93 ± 0.85
41	32	1.45 ± 0.09	2.17 ± 0.13	-0.73 ± 0.16
42	33	30.12 ± 0.29	19.74 ± 0.40	0.77 ± 0.04
43	34	0.42 ± 0.10	0.32 ± 0.05	0.47 ± 0.51
44	35	15.08 ± 0.24	9.59 ± 0.18	0.82 ± 0.04
45		0.20 ± 0.09	0.21 ± 0.05	-0.07 ± 0.92
46		0.50 ± 0.07	< 0.47	> 0.11
47		0.47 ± 0.09	0.27 ± 0.13	0.98 ± 0.92
48	36	0.54 ± 0.13	0.34 ± 0.10	0.82 ± 0.67
49A	37A	2.67 ± 0.13	1.83 ± 0.10	0.68 ± 0.13
49B	37B	6.68 ± 0.14	4.84 ± 0.10	0.58 ± 0.05
49	37	9.04 ± 0.19	6.66 ± 0.14	0.55 ± 0.05
50		0.28 ± 0.05	0.18 ± 0.05	0.81 ± 0.60
51	38	0.49 ± 0.09	0.37 ± 0.05	0.52 ± 0.42
52	39	2.06 ± 0.09	1.40 ± 0.12	0.70 ± 0.17
53	40	1.54 ± 0.10	1.79 ± 0.12	-0.28 ± 0.16
54	41	0.91 ± 0.18	0.68 ± 0.12	0.53 ± 0.48
55		0.31 ± 0.05	0.18 ± 0.06	0.99 ± 0.67
56	42	2.38 ± 0.13	1.87 ± 0.16	0.44 ± 0.18
57	43	1.71 ± 0.10	1.07 ± 0.10	0.85 ± 0.21
58	44	1.29 ± 0.12	0.91 ± 0.12	0.63 ± 0.30
	45	0.15 ± 0.05	0.33 ± 0.05	-1.42 ± 0.66
59		0.38 ± 0.07	0.30 ± 0.06	0.43 ± 0.52
60	46	0.94 ± 0.08	0.42 ± 0.12	1.46 ± 0.55
	47	< 0.28	0.31 ± 0.18	< -0.21
61		0.31 ± 0.06	< 0.20	> 0.74
62	48	0.45 ± 0.06	0.41 ± 0.13	0.19 ± 0.64
63		0.35 ± 0.11	< 0.28	> 0.38